

---

# Near-Ultraviolet Absorption Annealing in HfO<sub>2</sub> Thin Films Subjected to Continuous-Wave Laser Irradiation

## Introduction

Hafnium oxide is used in numerous applications as a high-index component in optical coatings for high-power lasers ranging from a near-infrared (IR) to near-ultraviolet (UV) light spectrum. It is also known that for the most frequently used film-pair combination of HfO<sub>2</sub>/SiO<sub>2</sub>, HfO<sub>2</sub> is the material in which nanosecond-pulse laser damage is initiated.<sup>1</sup> In this context, reduction of absorption in this material is crucial to improving damage performance of the coatings used in mirrors and other laser components. Previous studies<sup>2</sup> have shown that near-UV absorption in HfO<sub>2</sub> thin films is generated by high-spatial-density (an average separation of 100 nm or less) nanoscale absorbers whose nature is attributed to the agglomeration of electronic defects. Electronic defects exist even in high-quality optical bulk materials, such as crystals and glasses. In thin films, additional absorbing states might exist because of the presence of interfaces and grain boundaries. There are very limited ways to influence the concentration of the absorbing states once the thin film is deposited. Thermal annealing<sup>3,4</sup> is the process most frequently used as a research tool, but there are obvious practical limitations for optical parts used in large-scale lasers. Irradiation by pulsed laser radiation at fluences below damage threshold (also called laser conditioning) is another widely used method.

In this work we explore the possibility of using continuous-wave (cw)–laser radiation with power densities in the range of 50 kW/cm<sup>2</sup> to >1 MW/cm<sup>2</sup> to anneal absorption in HfO<sub>2</sub> monolayer films in the near-UV spectral range. We also investigate the absorption-annealing impact on pulsed-laser–damage behavior of HfO<sub>2</sub> monolayers subjected to irradiation by 351-nm, 0.9-ns pulses and 1053-nm, 600-fs pulses.

## Experimental

A HfO<sub>2</sub> monolayer film with a 180-nm physical thickness (one wave at 351 nm) was e-beam deposited on a fused-silica substrate on top of a 500-nm-thick SiO<sub>2</sub> film, isolating the HfO<sub>2</sub> film from the substrate defects introduced by the polishing process. The deposition rate was 1.2 Å/s and the oxygen pressure was  $8 \times 10^{-5}$  Torr. For monolayer absorption charac-

terization, we used a photothermal heterodyne imaging (PHI) technique, utilizing pump and probe laser beams focused onto a submicrometer spot on a sample having the same objective. Modulated pump-light absorption inside the sample produces a locally modulated refractive-index variation, which causes probe-light scattering amplified by far-field interference. Using the nanopositioning stage for the sample translation allows one to map absorption of the film sample with a better-than-0.4- $\mu$ m spatial resolution. A detailed description of the PHI technique principle and the setup used in this work are given in Refs. 2 and 5.

Near-UV, cw-laser–absorption annealing was studied using either a 351-nm, 1-W Ar<sup>+</sup> laser or a 355-nm, diode-pumped semiconductor laser that works as a pump laser for PHI and delivers up to 6 mW on the sample. The latter, after being focused into a  $\leq 0.7$ - $\mu$ m [full width at half maximum (FWHM)] spot by a 40 $\times$ /0.95 numerical-aperture (N.A.) objective, produced power densities of up to 1 MW/cm<sup>2</sup>, and the former was focused into a 50- $\mu$ m spot ( $1/e^2$ ), resulting in a 46-kW/cm<sup>2</sup> power density. A sample exposure, in the case of a small laser spot (PHI pump laser), was accomplished by using two different methods. In the first method, the sample position and laser power were fixed and the sample was exposed for some period of time, typically up to 15 min. In this manner, several sample sites were irradiated at a different cw-laser power. The second method consisted of raster-scanning the sample with typical velocities of 1 to 10  $\mu$ m/s, producing different exposures by varying the sample velocity and laser power. To quantify the exposure effect at a particular location, another raster scan of the larger area, including the exposed area, was performed with high sample velocity and low laser power to minimize additional energy deposition. In the case of a large laser spot (Ar<sup>+</sup> laser), the sample was translated in one direction with 1- $\mu$ m/s velocity, creating a 50- $\mu$ m-wide, several-mm-long exposed area.

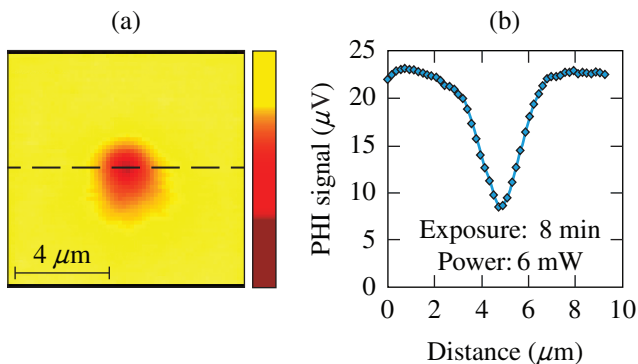
Laser-damage testing of cw-laser exposed and unexposed sample areas was performed in a 1-on-1 regime, using 351-nm, 0.9-ns pulses of a Nd:YLF diode-pumped laser<sup>6</sup> and 1053-nm, 600-fs, best-compression pulses from a laser using the standard

chirped-pulse–amplification scheme.<sup>7</sup> Damage testing using 0.9-ns pulses was conducted in an ambient environment and laser testing with 600-fs pulses was performed in a  $10^{-7}$ -Torr vacuum environment to avoid self-focusing in air. The laser-beam spot size ( $1/e^2$ ) on the sample was  $400\ \mu\text{m}$  and  $270\ \mu\text{m}$  for 0.9-ns and 600-fs beams, respectively. Laser-damage morphology was investigated by means of atomic force microscopy (AFM).

## Results and Discussion

### 1. Absorption-Annealing Effects

Figure 138.33 shows the result of irradiating  $\text{HfO}_2$  film for 8 min at a fixed location using a 355-nm, 6-mW beam focused into a submicrometer spot ( $\leq 0.7\text{-}\mu\text{m}$ ,  $\sim 1\text{-MW}/\text{cm}^2$  power density). Figure 138.33(a) is a PHI scan of a  $10 \times 10\text{-}\mu\text{m}^2$  film area centered around the location of the laser spot. A cross-sectional profile of the PHI signal [Fig. 138.33(b)] shows up to a 70% reduction in absorption within the irradiated spot, which appeared to be permanent when confirmed by PHI scans performed after one week and then one month later. Next, absorption annealing was investigated as a function of laser power and exposure time. Figure 138.34 plots a PHI signal's dependence on exposure time for three different values of laser-beam power: 0.7 mW, 3 mW, and 6 mW. One can see that the main drop in signal takes place during the first minute and is then followed by a slow decline on an  $\sim 10$ - to 15-min time scale. The initial signal drop becomes faster and deeper with increasing laser power. Nevertheless, the temporal behavior of the 6-mW and 3-mW curves shows that at long exposures, the signal can eventually be stabilized at the same level. It suggests that within some range of power densities, overall absorption reduction is proportional to both power density and exposure time or, in different terms, locally deposited energy.

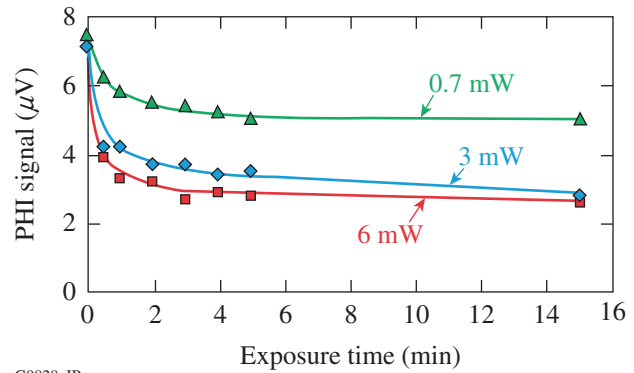


G9829aJR

Figure 138.33

(a) A photothermal heterodyne imaging (PHI) map of a  $10 \times 10\text{-}\mu\text{m}^2$  film area and (b) the signal horizontal profile through the central spot irradiated by a 355-nm, 6-mW cw laser for 8 min.

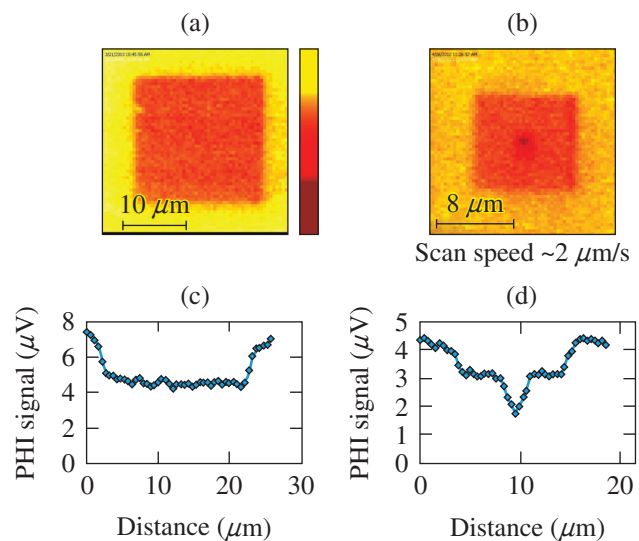
In an attempt to demonstrate the possibility of annealing absorption within a sample area larger than the laser spot, we performed square raster scans with linear dimensions of several tens of micrometers. Figure 138.35 shows corresponding PHI images, each obtained as a result of two scans. In the first image [Fig. 138.35(a)] the central  $20 \times 20\text{-}\mu\text{m}$  part was initially scanned with a high laser power of 4.5 mW and a low



G9828aJR

Figure 138.34

Temporal behavior of absorption as a function of cw-laser power on sample.



G9830aJR

Figure 138.35

PHI maps resulting from 355-nm cw-laser annealing by means of raster-scanning with a low,  $1\text{-}\mu\text{m}/\text{s}$  sample velocity: (a) a  $30 \times 30\text{-}\mu\text{m}^2$  area with the central  $20 \times 20\text{-}\mu\text{m}^2$  part exposed using 4.5-mW laser power; (b) a  $20 \times 20\text{-}\mu\text{m}^2$  area with the central  $10 \times 10\text{-}\mu\text{m}^2$  part raster-scan exposed, using 6 mW and, in addition, the central spot exposed for 8 min with 6-mW power; [(c) and (d)] horizontal signal profiles taken through the central part of the (a) and (b) maps, respectively.

scan velocity of  $\sim 1 \mu\text{m/s}$  to achieve the annealing effect. Subsequently, the larger square area ( $30 \times 30 \mu\text{m}^2$ ), with the same center coordinate, was imaged using a much lower laser power of 1.5 mW and a several-times-higher speed velocity, such that no, or very little, annealing effect was produced by the second scan. A cross-section horizontal-signal profile revealed at least a 40% reduction in absorption within the initially scanned area. A similar procedure was used for the  $20 \times 20\text{-}\mu\text{m}$  image shown in Fig. 138.35(b), with the only difference being that the central spot was exposed for an additional 8 min using 6 mW of laser power. In this case, the horizontal signal profile shows a 70% reduction in absorption in the central spot. From a practical point of view, it should be noted that because of the scan-velocity and beam-size limitations (the latter defines the maximum separation between two consecutive scan lines, or minimum number of lines per scan), raster-scanning for annealing purposes is very time consuming. For example, it takes at least 2 h to complete a  $60 \times 60\text{-}\mu\text{m}$  scan using a  $1\text{-}\mu\text{m/s}$  scan velocity.

The question to be addressed is the possibility of scaling up the absorption-annealing process for  $\text{HfO}_2$  films used in optical parts for laser applications. In this work, we explored the possibility of producing absorption annealing in a  $\text{mm}^2$ -scale area using a cw  $\text{Ar}^+$  laser having a maximum 351-nm output power of 1 W. In this case, a laser beam having a power of  $\sim 900$  mW was focused onto a  $50\text{-}\mu\text{m}$ -diam ( $1/e^2$ ) spot on the sample, which was slowly ( $\sim 1 \mu\text{m/s}$ ) linearly translated for a distance of 3.6 mm. Despite a much lower power maximum density of  $46 \text{ kW/cm}^2$ , as compared to  $\sim 1 \text{ MW/cm}^2$  in the case of a small PHI pump laser spot, a much longer (at least  $50\times$ ) exposure time allowed us to achieve an almost 50% absorption reduction (see Fig. 138.36) in the film area of  $\sim 0.2 \text{ mm}^2$ .

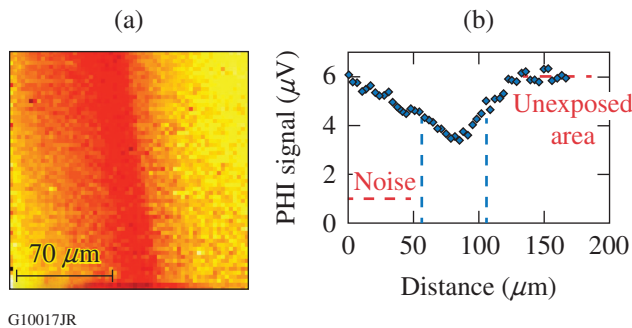


Figure 138.36  
(a) A  $180\text{-}\mu\text{m}$  PHI scan and (b) corresponding horizontal signal profile of the  $\text{HfO}_2$  film area irradiated by a  $900\text{-mW}$   $\text{Ar}^+$  laser. The sample vertical travel velocity was  $1 \mu\text{m/s}$ .

## 2. Laser-Damage Performance of Annealed $\text{HfO}_2$ Films

**a. Nanosecond-pulse damage.** Laser-damage performance of thin films is usually strongly linked to the absorption properties of the film material and, therefore, can provide a true measure of absorption annealing. In this work, damage thresholds and damage morphology were investigated for cw-laser-annealed film areas and then compared to the damage behavior of unexposed, as-produced film areas. As a starting point, we conducted AFM imaging of the cw-laser-annealed film columnar structure, which was then compared to the columnar structure of the unexposed film. High-resolution ( $\sim 7\text{-nm}$ ) AFM images of these two areas (see Fig. 138.37) revealed no modification caused by the near-UV, cw-laser exposure with power densities up to  $\sim 1 \text{ MW/cm}^2$ , implying that local heating of the material produced temperatures well below the  $\text{HfO}_2$  melting point.

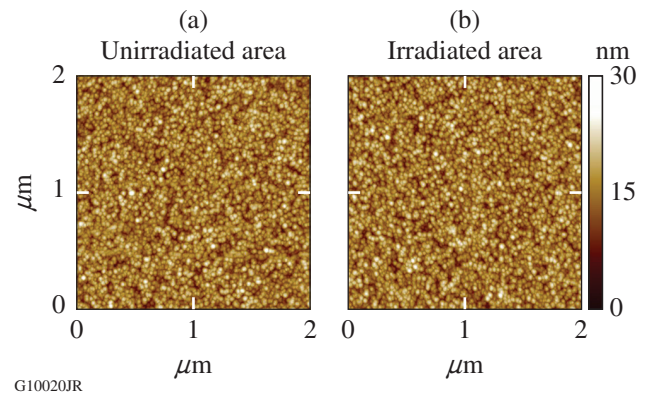


Figure 138.37  
Atomic force microscopy (AFM) images ( $2 \times 2 \mu\text{m}$ ) of cw-laser (a) unirradiated and (b) irradiated  $\text{HfO}_2$  film areas.

To evaluate the effect of absorption annealing on  $\text{HfO}_2$  film-damage resistance, a series of  $20 \times 20\text{-}\mu\text{m}$  cw-laser-exposed areas were produced on a sample and then irradiated by a pulsed laser (351 nm, 0.9 ns) at fluences exceeding damage threshold. Figure 138.38 depicts an optical micrograph of such a film area irradiated by a 351-nm, 0.9-ns pulse with a peak fluence  $\sim 30\%$  above the threshold. A square-shaped unaffected area where cw-laser exposure was carried out is clearly visible inside the damaged zone. Laser-fluence estimates show an  $\sim 25\%$  increase in damage threshold within the film area subjected to annealing, which unambiguously proves that absorption is reduced in cw-laser-exposed film.

A high-resolution AFM map (see Fig. 138.39) of the sample site, shown earlier in Fig. 138.38, provides additional information on annealing's impact on absorption sources in film material. Taking into account that damage morphology is rep-

resented by isolated craters, crater-depth distribution provides a rough approximation for the localized absorber distribution within the sample material. The crater-depth distribution was measured for the damage-site area adjacent to the exposed area [Fig. 138.39(b)], which should provide a reasonable estimate of the initial absorber distribution within the exposed material.

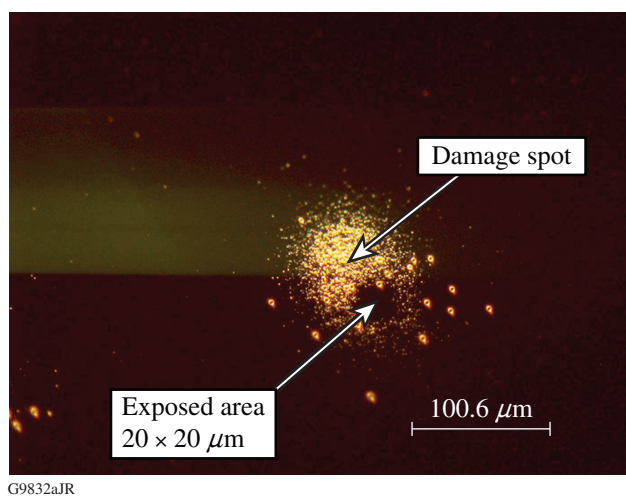
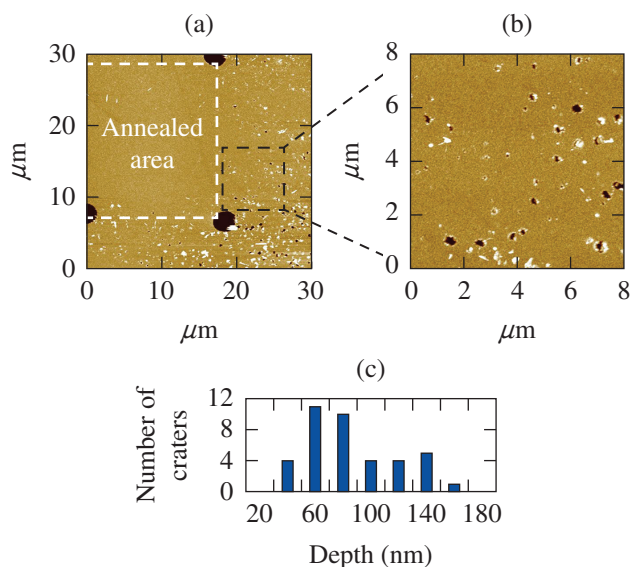


Figure 138.38

An optical micrograph of an  $\text{HfO}_2$  film site damaged by a 351-nm, 0.9-ns single pulse. Damage morphology clearly shows a damage-free,  $\sim 20 \times 20\text{-}\mu\text{m}^2$  square area subjected to exposure by a 6-mW, 355-nm cw laser.



G10016JR

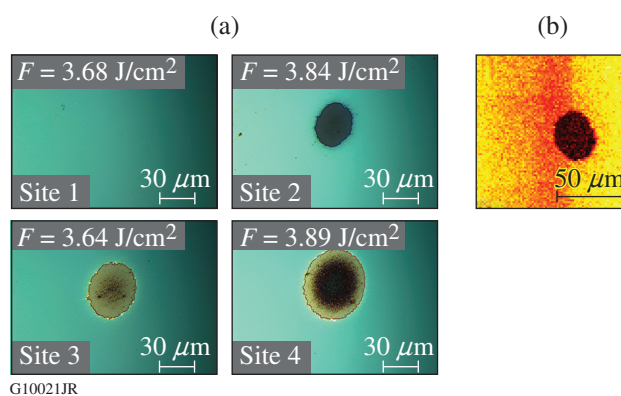
Figure 138.39

(a) A  $30 \times 30\text{-}\mu\text{m}$  AFM scan of a nanosecond-pulse damaged film site, including part of a cw-laser-exposed area. (b) A higher-resolution,  $8 \times 8\text{-}\mu\text{m}$  scan showing damage craters bordering an undamaged cw-laser-irradiated area. (c) Crater-depth distribution confirming the location of absorption sources inside the 180-nm-thick  $\text{HfO}_2$  film.

One can see that the crater depth does not exceed the 180-nm depth that equals the thickness of the  $\text{HfO}_2$  layer. This result indicates that annealed absorption precursors are indeed located inside  $\text{HfO}_2$  film and not in  $\text{SiO}_2$  film or the substrate.

**b. Short-pulse (600-fs) damage.** Previous studies<sup>8</sup> suggest that electronic defects might also play a role for short-pulse (picosecond, femtosecond) laser damage. In this context, the possible impact of the cw-laser annealing of the absorption precursors on short-pulse damage performance is of interest. Similar to the nanosecond-pulse study, near-UV, cw-laser irradiation of  $\text{HfO}_2$  film was conducted utilizing both a small spot ( $\leq 0.7\ \mu\text{m}$ ) of a PHI laser and a  $50\text{-}\mu\text{m}$  spot of an  $\text{Ar}^+$  laser. The results of 1053-nm, 600-fs-pulse damage testing of exposed (sites 1 and 2) and unexposed (sites 3 and 4) film areas are presented in Fig. 138.40, showing damage morphologies as recorded by an optical microscope. It is evident that the exposed sites show no damage at all while being irradiated by pulses with fluences above the unexposed film threshold of  $3.45\ \text{J}/\text{cm}^2$  (compare sites 1 and 3) or show a smaller extent of damage (site 2 versus site 4) as compared to the unexposed sites. Moreover, as evidenced by the PHI image of damaged site 2 [see Fig. 138.40(b)], the damaging pulse has partially missed the exposed area, which, in the case of a better overlap, could show an even larger difference in the damage scale for sites 2 and 4.

To summarize, near-UV, cw-laser annealing improves the damage resistance of e-beam-deposited  $\text{HfO}_2$  films to pulsed laser radiation at both 351 and 1053 nm.



G10021JR

Figure 138.40

(a) Optical micrographs of 600-fs-pulse damage morphology. Sites 1 and 2: cw-laser irradiated; sites 3 and 4: unirradiated. (b) PHI scan of site 2 showing relative positions of the cw-laser-irradiated area and damaging-pulse imprint.

### 3. Absorption-Annealing Mechanisms

Mechanisms of the near-UV, cw-laser annealing of absorption in HfO<sub>2</sub> films and related improvements in pulsed-laser-damage resistance may be explained if one considers electronic defects as a main source of absorption and damage initiation. Numerous types of defects can exist in HfO<sub>2</sub> bulk material with electronic energy levels located inside the bandgap<sup>9</sup> and even more are expected to exist for HfO<sub>2</sub> films caused by the columnar film structure. As suggested earlier,<sup>2</sup> in the case of near-UV, nanosecond-pulse damage, some of these states—as single- and double-ionized oxygen vacancies [V<sup>+</sup>, V<sup>2+</sup>, respectfully (see Fig. 138.41)]—are shallow enough that absorption of 351-nm photons (3.54 eV) can initiate transition of the electron into the conduction band. Further heating of these free electrons by the remaining laser pulse energy can promote electron-avalanche formation and damage. The same defect-energy levels might initiate multiphoton absorption and damage in the case of short, 600-fs pulses at 1053 nm. Assuming the validity of such a damage mechanism, the cw-laser-induced absorption-annealing effect and linked increase in pulsed-laser-damage resistance can be explained by depopulating the absorbing states.

The first possible scenario involves cw-laser-excited electron transition into the conduction band, where the electron spends time of the order of 10 ps (Ref. 8), followed by recombination with holes in the valence band or trapping into the deep defect states in the band gap, as shown in Fig. 138.41. Modeling this scenario using kinetic equations may provide further clarification of the annealing mechanism. This type of study, as well as extending the investigation of cw-laser anneal-

ing from monolayers to multilayer systems, should become the subject of future research.

The second absorption-annealing scenario may be linked to heating the film material resulting from absorption of UV-laser photons. Thermal annealing is widely used to improve the mechanical and optical performance of thin films, including laser-damage resistance in the near UV, as was recently demonstrated<sup>10</sup> for HfO<sub>2</sub> monolayer films at a 355-nm wavelength. In that work, the HfO<sub>2</sub> film temperature was increased by at least 100°C above room temperature to observe the absorption-annealing effect, with maximum effect obtained at an annealing temperature of 300°C. To evaluate possible thermal effects in our study, the temperature distribution in HfO<sub>2</sub> film was modeled with the assumption that all the energy absorbed in the film is released in the form of heat. The energy deposition was considered homogeneous in the cylindrical film volume with a diameter equal to the FWHM diameter of the laser beam (~600 nm) and a height equal to a 180-nm film thickness. The geometry of the model is shown in Fig. 138.42(a). The cw-laser intensity was fixed at 1 MW/cm<sup>2</sup> (highest used in the experiment), and the energy deposited in the film was varied by changing the film absorption in the range of 10 ppm (parts per million) to 1000 ppm, with an upper absorption boundary (1000 ppm) being well above the film absorption estimated from photothermal measurements. Heat conduction was considered to be the only channel of energy dissipation, and temperature rise in the film was obtained by solving appropriate heat-conduction equations:

$$\rho C \frac{\partial T}{\partial t} = \nabla \kappa \nabla T + S, \quad (1)$$

where  $\rho$ ,  $C$ , and  $\kappa$  are the density, heat capacity, and heat conductivity of the materials, respectively;  $T$  is the temperature; and  $S$  is the absorbed laser power per unit volume. The material parameters for modeling are listed in Table 138.VII. No reliable data are available for the heat capacity and density values for HfO<sub>2</sub> and SiO<sub>2</sub> films; for that reason, their values were set equal to the bulk values. It should be noted here that these parameters in the cw-laser regime affect only the time necessary to reach peak temperature but not the peak temperature value [as can be seen from Eq. (1) by setting the temperature derivative to zero]. A standard two-dimensional (2-D) cylindrical (five-point spatial), time-explicit finite-difference scheme was used to discretize and solve the heat-conduction equation (see, e.g., Chap. 8 of Ref. 11). The zero heat-flux boundary condition was applied at the film/air interface ( $z = 0$ ), and a zero-temperature boundary condition was applied at the other boundaries of the computational domain, which was chosen to be large enough to

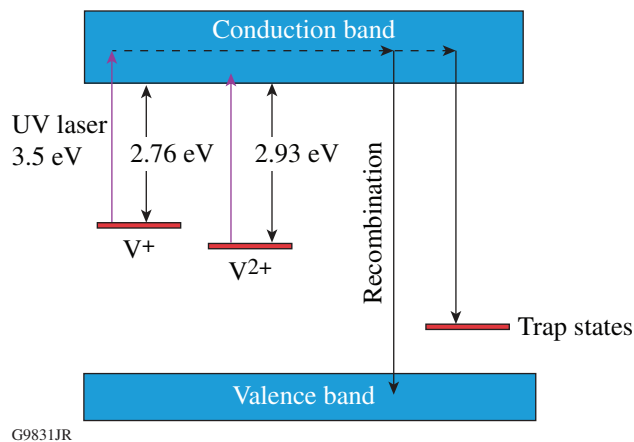
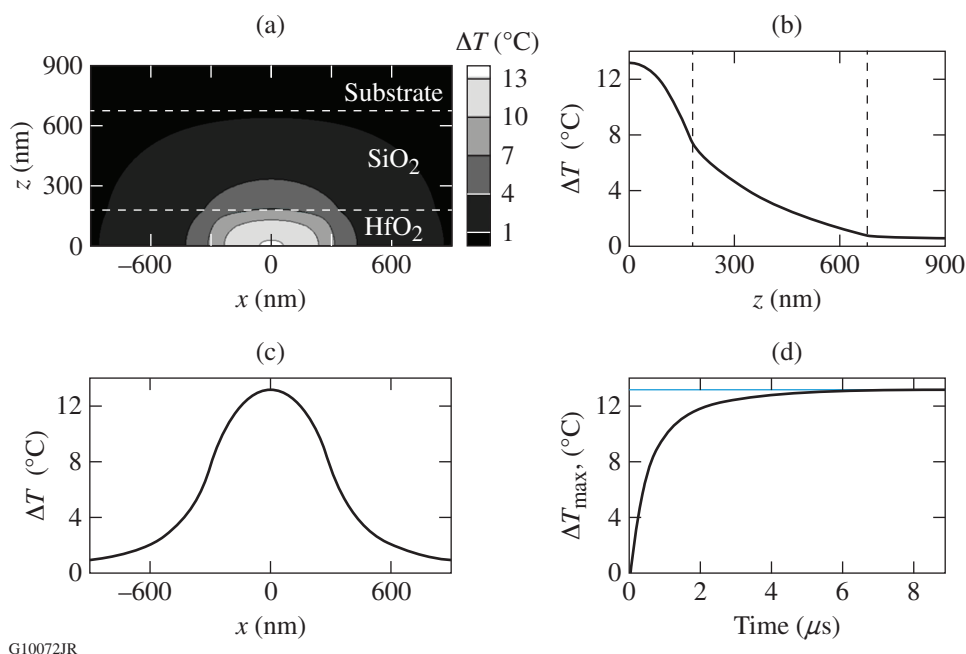


Figure 138.41  
HfO<sub>2</sub> energy-level diagram illustrating the possible mechanism of near-UV absorption annealing.



G10072JR

Figure 138.42

Peak temperature-rise distribution in a thin-film sample: (a) modeling geometry and distribution in  $x$ - $z$  plane ( $y = 0$ ); (b) lineout along  $z$  axis ( $y = x = 0$ ); (c) lineout along  $x$  axis ( $y = z = 0$ ); and (d) time evolution of the maximum temperature rise.

Table 138.VII: Parameters used to calculate the rise in HfO<sub>2</sub> film temperature.

	Thermal Conductivity (W/m·K)	Heat Capacity (J/kg·K)	Density (kg/m <sup>3</sup> )
HfO <sub>2</sub> film	0.10	287	9700
SiO <sub>2</sub> film	0.25	741	2200
Fused-silica substrate	1.38	741	2200

not affect the calculated temperature by more than 0.1°C. The modeling results presented in Fig. 138.42 show that at the highest chosen absorption level of 1000 ppm, the peak temperature rise does not exceed 14°C, which is not enough to produce the absorption-annealing effect. Two-dimensional temperature change distribution is shown in Fig. 138.42(a) along with its lineouts along the axis of symmetry  $z$  ( $x = y = 0$ ) in Fig. 138.42(b) and along the  $x$  axis ( $y = z = 0$ ) in Fig. 138.42(c). The time evolution of the maximum temperature rise, which is observed along the center of the laser beam at the HfO<sub>2</sub>/air interface,  $x = y = z = 0$ , after the laser is turned on at time  $t = 0$ , is shown in Fig. 138.42(d). It is worth noting that all these conditions lead to the highest-possible peak film-temperature estimates. Adding energy dissipation channels (such as luminescence or structural transformations) would lead to lower peak tempera-

tures. Consequently, one can conclude that depopulation of the absorbing states is not caused by heat-induced structural matrix transformation.

Finally, it should be noted that irradiation of thin films by cw lasers with power densities used in this work can produce different absorption-modification effects. For instance, in similar experimental conditions,<sup>12</sup> irradiation of TiO<sub>2</sub> monolayer films using an 800-nm cw laser caused an increase in absorption that was also dependent on exposure time. Consequently, absorption-modification effects are thin-film material and cw-laser wavelength specific.

## Conclusions

Irradiation of e-beam-deposited HfO<sub>2</sub> monolayer films by near-UV, cw-laser light with power densities of 50 kW/cm<sup>2</sup> to 1 MW/cm<sup>2</sup> produced significant modification of near-UV film absorption. A reduction in absorption as high as 70% was achieved in film areas subjected to exposure. The effect is permanent, as confirmed by repeated measurements over a several-month period. It has been shown that absorption modification is achieved without any changes in the film's columnar structure on a spatial scale of up to a few nanometers. This led to the conclusion that a reduction of absorption is linked to the modification of the atomic film structure—in particular, to changes in the concentration of structural

defects responsible for near-UV absorption. Investigation of 351-nm, ns-pulse laser-damage behavior of  $\text{HfO}_2$  monolayer films subjected to cw-laser exposure showed a >25% increase in damage thresholds and confirmed that absorption can be reduced by annealing the absorbing defects residing inside the  $\text{HfO}_2$  film. Short, 600-fs pulse irradiation also indicated an increase in laser-damage resistance of cw-laser-exposed areas as compared to unexposed areas. This result suggests partial cw-laser annealing of electronic defects participating in the multiphoton absorption process that initiates damage by 600-fs pulses. Future research will concentrate on further clarification of the annealing mechanism and will extend the study to multilayer systems.

#### ACKNOWLEDGMENT

This material is based upon work supported by the Department of Energy National Nuclear Security Administration under Award Number DE-NA0001944, the University of Rochester, and the New York State Energy Research and Development Authority. The support of DOE does not constitute an endorsement by DOE of the views expressed in this article.

#### REFERENCES

1. S. Papernov and A. W. Schmid, *J. Appl. Phys.* **82**, 5422 (1997).
2. S. Papernov, A. Tait, W. Bittle, A. W. Schmid, J. B. Oliver, and P. Kupinski, *J. Appl. Phys.* **109**, 113106 (2011).
3. M. Tilsch, V. Scheuer, and T. T. Tschudi, in *Optical Thin Films V: New Developments*, edited by R. L. Hall (SPIE, Bellingham, WA, 1997), Vol. 3133, pp. 163–175.
4. G. Tian *et al.*, *Appl. Surf. Sci.* **239**, 201 (2005).
5. S. Berciaud *et al.*, *Phys. Rev. B* **73**, 045424 (2006).
6. A. V. Okishev, I. A. Begishev, R. Cuffney, S. Papernov, and J. D. Zuegel, in *Solid State Lasers XXII: Technology and Devices*, edited by W. A. Clarkson and R. Shori (SPIE, Bellingham, WA, 2013), Vol. 8599, Paper 85990Q.
7. H. P. Howard, A. F. Aiello, J. G. Dressler, N. R. Edwards, T. J. Kessler, A. A. Kozlov, I. R. T. Manwaring, K. L. Marshall, J. B. Oliver, S. Papernov, A. L. Rigatti, A. N. Roux, A. W. Schmid, N. P. Slaney, C. C. Smith, B. N. Taylor, and S. D. Jacobs, *Appl. Opt.* **52**, 1682 (2013).
8. D. N. Nguyen *et al.*, *Appl. Phys. Lett.* **97**, 191909 (2010).
9. A. S. Foster *et al.*, *Phys. Rev. B* **65**, 174117 (2002).
10. S. Kičas *et al.*, in *Laser-Induced Damage in Optical Materials: 2013*, edited by G. J. Exarhos *et al.* (SPIE, Bellingham, WA, 2013), Vol. 8885, Paper 888521.
11. R. D. Richtmyer and K. W. Morton, *Difference Methods for Initial-Value Problems*, 2nd ed. (Interscience, New York, 1967).
12. W. Rudolph *et al.*, in *Laser-Induced Damage in Optical Materials: 2013*, edited by G. J. Exarhos *et al.* (SPIE, Bellingham, WA, 2013), Vol. 8885, Paper 888516.